

Predictive-Integral Current Controller for Active- and Reactive-Power Control of Wind Generators

Pedro Roncero-Sánchez¹, Vicente Feliu¹ and Aurelio García-Cerrada²

¹Department of Electrical, Electronics, Control Engineering and Communications

E.T.S. Ingenieros Industriales, Universidad de Castilla-La Mancha

Avda. Camilo José Cela S/N, 13071, Ciudad Real, (Spain)

Phone:+34 926 29 53 00. e-mail: **Pedro.Roncero@uclm.es**, **Vicente.Feliu@uclm.es**

²Department of Electronics and Control Engineering

E.T.S. de Ingeniería ICAI, Universidad Pontificia Comillas

C/ Alberto Aguilera 23, 28015, Madrid, (Spain)

Phone:+34 91 542 28 00. e-mail: **aurelio@iit.upcomillas.es**

Abstract

This paper deals with the design of a predictive-integral current controller for wind generators connected to the grid. The goal is to achieve a decoupled control of d- and q-axes current components at the connection point, which results in a decoupled control of the active and the reactive power exchanged between the generator and the grid. Furthermore, the control system is designed in order to achieve a deadbeat closed-loop system. The robustness of the closed-loop dynamic response and the active and reactive-power coupling when system-modelling errors exist are studied. Simulation and experimental results will be presented to validate the main contributions of this work.

Key words

Wind generator, voltage-source converter, deadbeat system, predictive control, robust control

1 Introduction

Electricity generation making use of renewable energy sources has experienced a great growth in the last few years [1]. Wind generators are, probably, the clearest examples of this upgrowth. These systems must transfer the energy efficiently to the utility or to the load while supplying the necessary reactive power. For this purpose, current-controlled voltage-source electronic converters are normally used.

Current-control schemes can be classified into two main groups (see [2] and [3] for more details):

1. Linear control schemes with conventional pulse-width modulators that split current-control and modulation parts. This group comprises the PI average-mode controllers and also predictive and deadbeat control schemes.

2. Non-linear control schemes, including hysteresis-based controllers, pulse density modulation and also neural-network-based and fuzzy-logic controllers.

Predictive current controllers are recently being proposed very often in the literature: in this kind of controllers, the converter-output voltage is calculated in order to make the measured current to track the reference based on a predictive model [4]. The implementation of these current controllers is not ideal due to factors such as modelling errors or dead-time effects [5], which may substantially affect the dynamic performance or even cause instability problems. These issues have motivated this work.

Predictive current controllers applied to power-electronic converters can be found in [6–9]: in [6] a robust current controller is designed to obtain a dead-beat system for active filters and PWM rectifiers and a study of the robustness when there are modelling errors in the inverter-output inductance is included. Reference [7] deals with a predictive-current regulator applied to an induction-motor control. It also studies the effects of errors in some parameters on the dynamic performance. In [8] a dead-beat current controller for converters with both, variable or fix output frequency is developed. It uses an error law for the measured current which improves the stability when there are modelling errors in the load inductance. Finally, in [9], a predictive-current controller design for single-phase voltage-source converters connected to the grid is presented. A study of the robustness to the connection-inductance mismatch is included.

The present work deals with the design of a predictive-integral current controller to implement active- and reactive-power control in a wind generator, obtaining a decoupled dead-beat closed-loop system. Unlike the previous predictive-current controllers, an integral ac-

tion is added in order to guarantee zero tracking error in steady state for step changes in the reference, even when there are parameter errors. The dynamic performance is also studied.

The paper is organised as follows. A discrete decoupled model of the wind-generation system is obtained in Section 2. Section 3 explains the design for the predictive-integral controller. The stability limits of the closed-loop system when there are errors in the system parameters and how these parameter-errors affect the system dynamic and d - and q -axis coupling are studied in Section 4. In Section 5, the main results are tested through experimentation with a prototype. Finally, some conclusions are given in Section 6.

2 Model of the grid-connection system

Fig. 1 shows a possible configuration, among others, of wind generator. The main elements are: an induction machine driven by a wind turbine, the generator-side converter, the grid-side converter (the two converters share the D.C. link and they are two-level voltage-source converters) and an inductive filter plus a transformer at the grid side.

The generator-side converter controls the wind generator, resulting in a real power p_g flowing into the d.c.-link capacitor. At the same time, the grid-side converter controls the active power flowing into the grid (p) and the reactive power required (q). There are several options for the control of the induction generator according to the operation specifications: from a simple Indirect Field-Orientated Control (IFOC) scheme to a more sophisticated control scheme.

As the real power going into the capacitor p_c is equal to $p_g - p$, the equation $p_g = p$ must be fulfilled in steady-state if the average value of the capacitor voltage has to remain constant. Although losses have been neglected, closed-loop control of the d.c.-link voltage should take care of them.

Fig. 2 shows the single-phase equivalent circuit of the grid-side converter connected to the electrical grid, where the converter has been modelled as an ideal voltage source u , v is the grid voltage, i stands for the current injected into the grid, and r and L are, respectively, the resistance and the inductance that model the filter plus the transformer. In this paper the three-phase connection system is supposed to be

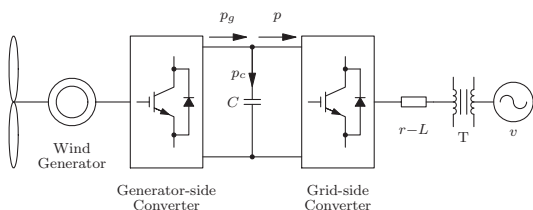


Fig. 1: Wind generator system

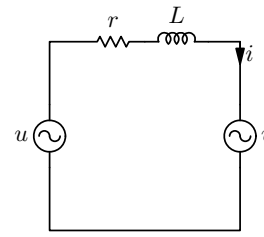


Fig. 2: Single-phase equivalent circuit of the converter connected to the grid

balanced.

The state-variable model of the three-phase system can be written by using the Park's Transformation (see [10]) with a reference frame rotating with the frequency of the grid voltage:

$$\frac{d}{dt} \begin{bmatrix} i_d \\ i_q \end{bmatrix} = \underbrace{\begin{bmatrix} -\frac{r}{L} & \omega \\ -\omega & -\frac{r}{L} \end{bmatrix}}_{\mathbf{A}} \underbrace{\begin{bmatrix} i_d \\ i_q \end{bmatrix}}_{\mathbf{i}_{d,q}} + \underbrace{\begin{bmatrix} \frac{1}{L} & 0 \\ 0 & \frac{1}{L} \end{bmatrix}}_{\mathbf{B}} \underbrace{\begin{bmatrix} u_d - v_d \\ u_q - v_q \end{bmatrix}}_{\mathbf{u}_{d,q} - \mathbf{v}_{d,q}} \quad (1)$$

where i_d and i_q are, respectively, the d and q components of the current (i), u_d and u_q are the inverter-output voltage components, v_d and v_q are the grid voltage components, and ω is the angular speed of the rotating frame used for the Park's Transformation. Note that the Park's transformation converts all sinusoidal variables of frequency ω into d.c. magnitudes.

By using a power-invariant Park's transformation, and by choosing the rotating reference frame so that the v_q component is always zero in (1), the instantaneous real power, p , and the instantaneous reactive power, q injected into the grid by the converter are [11]:

$$p = v_d i_d + v_q i_q = v_d i_d \quad (2)$$

$$q = -v_d i_q + v_q i_d = -v_d i_q \quad (3)$$

Hence p and q can be controlled by i_d and i_q components, respectively, and active- and reactive-power control is reduced to two current controllers. The control inputs in (1) are u_d and u_q , while v_d is a disturbance which can be measured.

The eigenvalues of the matrix \mathbf{A} in (1) are $\lambda_{1,2} = -\frac{r}{L} \pm j\omega$ with $j = \sqrt{-1}$. The eigenvectors associated with these are the columns of matrix \mathbf{V} as follows:

$$\mathbf{V} = \begin{bmatrix} 1 & -j \\ -j & 1 \end{bmatrix} \quad (4)$$

Gathering d and q components in column vectors with subscripts " \mathbf{d}, \mathbf{q} " and introducing vector $\mathbf{x}_{d,q}$ so that $\mathbf{i}_{d,q} = \mathbf{V}\mathbf{x}_{d,q}$, the following system is obtained:

$$\frac{d\mathbf{x}_{d,q}}{dt} = \underbrace{\mathbf{V}^{-1}\mathbf{A}\mathbf{V}}_{\mathbf{A}} \mathbf{x}_{d,q} + \mathbf{V}^{-1}\mathbf{B}(\mathbf{u}_{d,q} - \mathbf{v}_{d,q}) \quad (5)$$

with:

$$\mathbf{A} = \begin{bmatrix} -\frac{r}{L} + j\omega & 0 \\ 0 & -\frac{r}{L} - j\omega \end{bmatrix}, \text{ and } \mathbf{B} = L^{-1}\mathbf{I} \quad (6)$$

Since $\mathbf{V}^{-1}\mathbf{B} = \mathbf{B}\mathbf{V}^{-1}$ and by using the changes of variables $\mathbf{u}'_{d,q} = \mathbf{V}^{-1}\mathbf{u}_{d,q}$ and $\mathbf{v}'_{d,q} = \mathbf{V}^{-1}\mathbf{v}_{d,q}$, a fully decoupled system can be written as:

$$\frac{d\mathbf{x}_{d,q}}{dt} = \mathbf{A}\mathbf{x}_{d,q} + \mathbf{B}(\mathbf{u}'_{d,q} - \mathbf{v}'_{d,q}) \quad (7)$$

As the controller is implemented in a microprocessor based system, a discrete-time model of (7) must be obtained. If ω is constant, (7) is a linear-time-invariant model and the discrete-time system which gives exact results at the sampling times [12] is:

$$\begin{bmatrix} x_d \\ x_q \end{bmatrix}_{k+1} = \underbrace{\begin{bmatrix} a_d & 0 \\ 0 & a_q \end{bmatrix}}_{\mathbf{A}_c} \begin{bmatrix} x_d \\ x_q \end{bmatrix}_k + \underbrace{\begin{bmatrix} b_d & 0 \\ 0 & b_q \end{bmatrix}}_{\mathbf{B}_c} \begin{bmatrix} u'_d - v'_d \\ u'_q - v'_q \end{bmatrix}_k \quad (8)$$

where x_d and x_q are the state variables, u'_d and u'_q are the control inputs, and v'_d and v'_q are measured inputs. The coefficients (a_d, a_q) and (b_d, b_q) are pairs of complex conjugated numbers and matrices \mathbf{A}_c and \mathbf{B}_c are calculated as:

$$\mathbf{A}_c = e^{\mathbf{A}t_s}, \quad \mathbf{B}_c = \left(\int_0^{t_s} e^{\mathbf{A}t} dt \right) \mathbf{B} \quad (9)$$

t_s being the sampling interval.

System (8) gives the value of the state variables at instant $k + 1$ based on the values of the state variables and the inputs at instant k . As the controller may use a large part of the sampling time to calculate the system input from references and measurements, a reasonable assumption is to consider that the system input at instant k is the one calculated by the controller using measurements up to instant $k - 1$. In order to include this issue in the model [13], two new state variables are added to (8) to account for the control-calculated outputs (u'^*_d and u'^*_q) so that $u'_d(k) = u'^*_d(k - 1)$ and $u'_q(k) = u'^*_q(k - 1)$.

Finally, taking these new added state variables into account, system (8) can be written as:

$$\begin{bmatrix} x'_n \\ u'_n \end{bmatrix}_{k+1} = \begin{bmatrix} a_n & b_n \\ 0 & 0 \end{bmatrix} \begin{bmatrix} x'_n \\ u'_n \end{bmatrix}_k + \begin{bmatrix} 0 & -b_n \\ 1 & 0 \end{bmatrix} \begin{bmatrix} u'^*_n \\ v'_n \end{bmatrix}_k \quad (10)$$

where subscript n stands for d and q axes.

3 Design of the control system

The predictive-current controller designed here includes an integral action to guarantee zero tracking error in steady state for step changes in the reference.

Taking (10) into account, the proposed control law is:

$$u'^*_n(k) = \frac{1}{b_n} x^*_n(k) - \frac{\hat{a}_n}{b_n} \hat{x}_n(k+1) + \hat{v}'_n(k+1) + g_n(k) \quad (11)$$

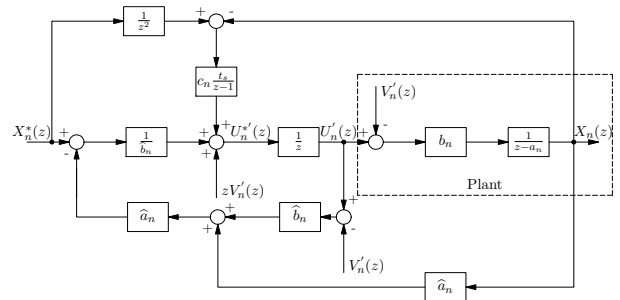


Fig. 3: Predictive-Integral control scheme

$$g_n(k+1) = g_n(k) + c_n t_s [x_n^*(k-2) - x_n(k)] \quad (12)$$

where $\hat{x}_n(k+1)$ and $\hat{v}_n(k+1)$ are the predicted values for x_n and v_n , respectively, at $k+1$ based on the information up to k , g_n is the integral of the error between the reference input x_n^* and the system output, and c_n weights that integral action. In addition \hat{a}_n and \hat{b}_n are the estimated values of the model parameters.

A very reasonable assumption for $\hat{v}_n(k+1)$ is to consider constant main voltage so that $\hat{v}_n(k+1) = v'_n(k)$, which is exactly true if an infinite bus system is considered. Moreover, the predicted value $\hat{x}_n(k+1)$ can be obtained by using (10) as prediction model:

$$\hat{x}_n(k+1) = \hat{a}_n x_n(k) + \hat{b}_n u'_n(k) - \hat{b}_n v'_n(k) \quad (13)$$

By applying the Z transform, the new closed-loop-system output is:

$$X_n(z) = F_n(z) X_n^*(z) \quad (14)$$

where:

$$F_n(z) = \frac{1}{z^2} \left[\frac{\frac{b_n}{b_n} z^2 (z-1) + b_n c_n t_s}{D_f(z)} \right] \quad (15)$$

with

$$D_f(z) = (z + \hat{a}_n)(z - \hat{a}_n)(z - 1) + \frac{b_n}{b_n} \hat{a}_n^2 (z - 1) + b_n c_n t_s \quad (16)$$

Note that if (15) is closed-loop asymptotically stable, the static gain is always $F_n(1) = 1$. Furthermore, if there are no modelling errors the closed-loop system is a second order deadbeat system $F_n(z) = 1/z^2$.

The block diagram of the whole control system is shown in Fig. 3.

4 Performance with parameter errors

The dynamic performance of the closed-loop system can be affected by several factors such as modelling errors in the parameters of the filter and the transformer, among others. For that reason, the robustness of the control scheme to modelling errors in the resis-

tance r and the inductance L has been investigated regarding the two aspects described below.

If the parameters used for design purposes are L_n and r_n and the actual filter values are L and r , it can be written:

$$r = r_n + \Delta r \quad (17)$$

$$L = L_n + \Delta L \quad (18)$$

with Δr and ΔL the parameter errors.

A. Stability

The stability of the closed-loop system has been investigated for $-r_n \leq \Delta r \leq r_n$ and $-L_n \leq \Delta L \leq L_n$ by calculating the closed-loop transfer-function poles. The region for which the closed-loop system remains stable for the prototype considered has been shadowed in Fig. 4 for two different values of c_n in (12).

The closed-loop system is stable for all resistance values specified in (17) and $0.475L_n \leq L \leq 2L_n$ when $c_n = 25 \cdot 10^3$, as it is shown in Fig. 4(a). Nevertheless, the stability region is reduced dramatically as c_n is increased. As an example, Fig. 4(b) shows the stability region for $c_n = 120 \cdot 10^3$. Further simulations show similar stability regions for $0 \leq c_n \leq 25 \cdot 10^3$.

B. Transient response

The control system was designed to achieve a dead-beat response in both axes without overshoot and with no coupling between them. However, the transient response deteriorates when r and L are different to the expected ones (see (17) and (18)).

Taking into account that $\mathbf{x}_{d,q} = \mathbf{V}^{-1}\mathbf{i}_{d,q}$ and $\mathbf{x}_{d,q}^* = \mathbf{V}^{-1}\mathbf{i}_{d,q}^*$, the system output can be calculated as $\mathbf{i}_{d,q} = \mathbf{F}_{i_{d,q}}(z)\mathbf{i}_{d,q}^*$, where:

$$\overbrace{\begin{bmatrix} F_{11}(z) & F_{12}(z) \\ F_{21}(z) & F_{22}(z) \end{bmatrix}}^{\mathbf{F}_{i_{d,q}}(z)} = \mathbf{V} \begin{bmatrix} F_d(z) & 0 \\ 0 & F_q(z) \end{bmatrix} \mathbf{V}^{-1} \quad (19)$$

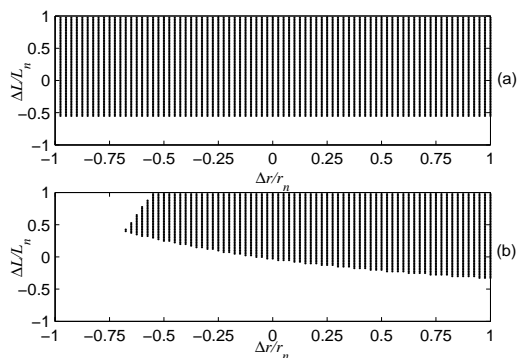


Fig. 4: Closed-loop stability with $r_n = 1.5 \Omega$ and $L_n = 23.3 \text{ mH}$ and: (a) $c_n = 25 \cdot 10^3$, and (b) $c_n = 120 \cdot 10^3$

The responses to a unit step at the set-point of systems $F_{11}(z)$ and $F_{22}(z)$ have been investigated by calculating the overshoot (M_p), and the 1%-settling time (t_{set}). Simulations have been carried out for $0.475L_n \leq L \leq 2L_n$ and $0 \leq r \leq 2r_n$.

The overshoot in % is plotted in Figs. 5(a)-(b) for $c_{n1} = 25 \cdot 10^3$ and $c_{n2} = 10 \cdot 10^3$, respectively. The worst value shows $M_p = 109.1\%$ for $L = 0.5L_n$ in both cases. However, for $L = 2L_n$, the overshoot diminishes as the value of the coefficient c_n decreases: from $15.9\% \leq M_p \leq 21.6\%$, for $c_{n1} = 25 \cdot 10^3$, to $4.3\% \leq M_p \leq 8.1\%$ for $c_{n2} = 10 \cdot 10^3$ (see Table 1).

Figs. 6(a)-(b) show the settling time obtained for $c_{n1} = 25 \cdot 10^3$ and $c_{n2} = 10 \cdot 10^3$, respectively. The lower the coefficient c_n is, the greater the settling time is, as it can be seen in Table 1. The worst values are found for the lowest inductance value ($L = 0.475L_n$).

The results shown in Figs. 5(a)-(b), Figs. 6(a)-(b), and Table 1, reveal that coefficient c_n must be chosen carefully to achieve a good dynamic performance. In this paper, c_{n2} is the one which provides the best performance and has been used in the rest of the work.

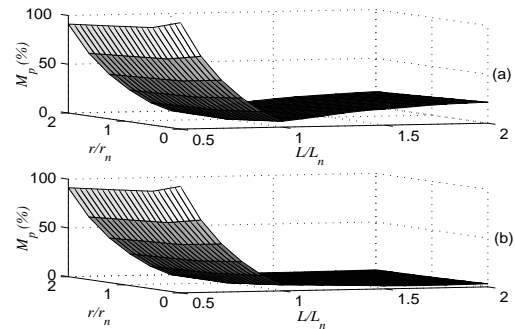


Fig. 5: Overshoot obtained with: (a) $c_{n1} = 25 \cdot 10^3$, and (b) $c_{n2} = 10 \cdot 10^3$

Table 1: Minimum and maximum values of the overshoot (M_{pmin} , M_{pmax}) and the settling time ($t_{set min}$, $t_{set max}$) obtained for several coefficients c_n

M_p and t_{set}/t_s obtained with $0 \leq r \leq 2r_n$			
c_n	$L = 0.475L_n$	$L = L_n$	$L = 2L_n$
M_p (%)			
$25 \cdot 10^3$	(91.1, 109.1)	(0.4, 6.1)	(15.9, 21.6)
$10 \cdot 10^3$	(91.1, 109.1)	(0.0, 6.1)	(4.3, 8.1)
t_{set}/t_s (No. of samples)			
$25 \cdot 10^3$	(48, 71)	(2, 9)	(37, 41)
$10 \cdot 10^3$	(62, 71)	(2, 20)	(44, 46)

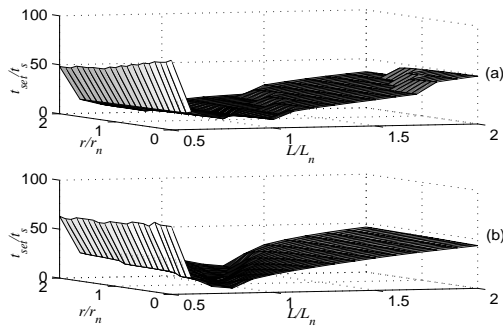


Fig. 6: Settling time in number of samples: (a) $c_{n_1} = 25 \cdot 10^3$, and (b) $c_{n_2} = 10 \cdot 10^3$

C. Coupling of the closed-loop system

In order to quantify the d - and q - axis coupling of the closed-loop system (see [14]), the impulse-response variance of the system $F_{12}(z)$ (equivalent to that one obtained with $F_{21}(z)$) has been analysed. This variance has been calculated as [15]:

$$I = \frac{1}{2\pi j} \oint H(z)H(z^{-1}) \frac{dz}{z} \quad (20)$$

where $H(z)$ stands for the transfer functions $F_{12}(z)$ or $F_{21}(z)$, j is the imaginary unit, and the factor $1/2\pi$ is introduced for scaling.

Fig. 7 shows the integral value I : the coupling is almost independent of the resistance modelling error, and the worst case is found for $L = 0.475L_n$, with $5.54 A^2 \leq I \leq 6.58 A^2$, whereas for $L = 2L_n$ the value range for the index is $0.013 A^2 \leq I \leq 0.017 A^2$.

5 Experimental results

The control scheme has been implemented on a PC using the Matlab Real-Time-Workshop. The prototype consists of a wind-generation system such as that depicted in Fig. 1 where only the grid converter has been used to test the performance of the controller. A 2.2 kW three-phase voltage-source converter (IR-MDAC3) has been used. The switching frequency and the sampling frequency have been set to 1050 Hz and 2100 Hz, respectively. The filter and the transformer have been modelled by $r = 1.5 \Omega$ in series

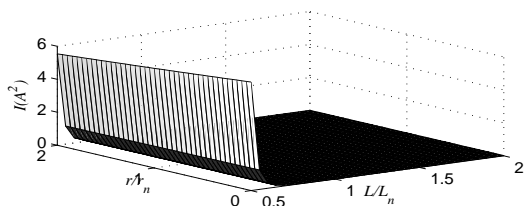


Fig. 7: Value of the integral I in A^2

with $L = 23.3$ mH. The grid line-to-line voltage was $v_{LL} = 400$ V, and the grid frequency was $f = 50$ Hz.

Let L_m be the inductance value used in the control design. To obtain a mismatch in the inductance and assuming that $L \approx L_n$, L_m has been modified from its nominal value, L_n , so that $0.5L_m \leq L \leq 2L_m$.

The current references change as follows: i_d^* changes from 0 to 2 A at $t = 0.5$ s and i_q^* changes from 0 to -1 A at $t = 0.6$ s. Coefficient c_n was set to $10 \cdot 10^3$.

Fig. 8(a) plots the responses of the currents i_d and i_q obtained without modelling errors: the currents are fully decoupled; there is no overshoot and no steady-state error. Fig. 8(b) shows the active ($p = 800$ W) and reactive ($q = 400$ VAR) powers injected into the electrical grid. If Figs. 8(a) and 8(b) are compared, it will be noted that p and q are proportional to the currents i_d and i_q , respectively. A detail of the current i_d is shown in Fig. 8(c), where the dead-beat response can be seen. Finally Fig. 8(d) shows a detail of the line current.

In order to study the controller performance close to its stability limits, two tests have been performed for $L_m = 2L$ and $L_m = 0.5L$. Figs. 9(a)-(b) show the results when $L_m = 2L$: the poor responses of the currents i_d and i_q are shown in Fig. 9(a) ($M_p = 99.7\%$ with a strong coupling between axes). Fig. 9(b) plots the response of the line current, which shows significant oscillations until the steady-state is reached. Figs. 9(c)-(d) show the results for $L_m = 0.5L$. The

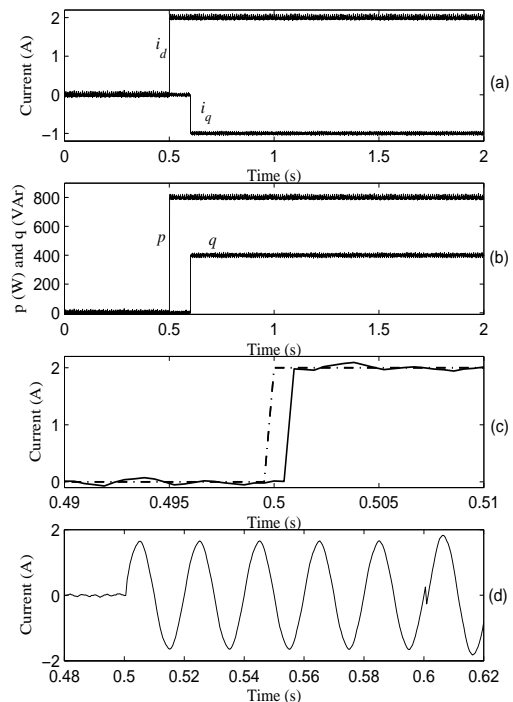


Fig. 8: Time response of (a) the current components and (b) active and reactive powers injected into the grid. (c) Detail of the current i_d : (---) reference, and (—) measured current. (d) Detail of the measured line current i_R

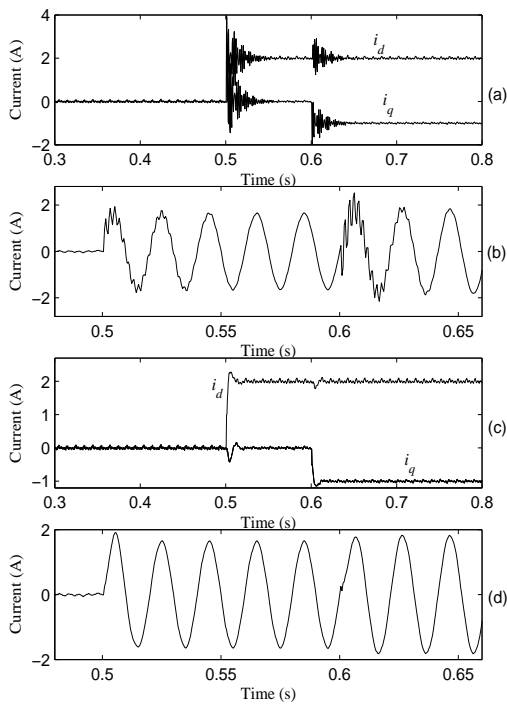


Fig. 9: Experimental results. $L_m = 2L$: (a) $d - q$ current components, and (b) detail of the measured line current i_R . $L_m = 0.5L$: (c) $d - q$ current components, and (d) detail of the measured line current i_R

responses of the currents i_d and i_q show better behaviour than in the previous case ($M_p = 14\%$ with a smaller $d - q$ coupling).

6 Conclusions

Nowadays, power-electronic converters are used to provide flexible active- and reactive-power control of wind generators connected to the grid, which is eventually seen as d - and q -axis current control.

This paper studies a predictive-integral current controller for PWM voltage-source converters connected to the grid. Unlike other classical control schemes which may exhibit a time response with overshoot or with non-zero error in steady-state, this control system has shown very good transient and steady-state performances when the system parameters are known exactly (the steady-state is reached in two sampling periods without overshoot and with zero tracking error), but the paper has also revealed that the performance deteriorates when there are modelling errors in the parameters of the connection impedance. The paper has studied how the closed-loop performance is affected by these errors: the system damping deteriorates and d - and q -axis dynamics are coupled.

The closed-loop system is robust for a wide range of parameter errors. Moreover, it is proved that high values of the integral-weighting coefficient improve the speed of the closed-loop response, but deteriorates the damping and the cross-coupling between axes.

The main contributions have been validated by means of simulation and experimental results in a prototype.

Acknowledgements

This work has been partially supported by the Castilla-La Mancha Council under research project PBI-06-0150.

References

- [1] T. Burton, D. Sharpe, N. Jenkins, and E. Bossanyi, *Wind Energy Handbook*. Chichester: John Wiley & Sons, Ltd, 2001.
- [2] L. Malesani and P. Tomasin, "PWM current control techniques of voltage source converters - a survey," in *Proceedings of the IECON '93*, vol. 2. IEEE, Nov. 1993, pp. 670–675.
- [3] M. P. Kazmierkowski and L. Malesani, "Current control techniques for three-phase voltage-source PWM converters: a survey," *IEEE Trans. Ind. Electron.*, vol. 45, no. 5, pp. 691–703, Oct. 1998.
- [4] S. J. Henriksen, R. E. Betz, and B. J. Cook, "Digital hardware implementation of a current controller for IM variable-speed drives," *IEEE Trans. Ind. Appl.*, vol. 35, no. 5, pp. 1021–1029, Sept./Oct. 1999.
- [5] T. J. Summers and R. E. Betz, "Dead-time issues in predictive current control," *IEEE Trans. Ind. Appl.*, vol. 40, no. 3, pp. 835–844, May/June 2004.
- [6] L. Malesani, P. Mattavelli, and S. Buso, "Robust dead-beat current control for PWM rectifiers and active filters," *IEEE Trans. Ind. Appl.*, vol. 35, no. 3, pp. 613–620, May/June 1999.
- [7] H. Abu-Rub, J. Guziński, Z. Krzeminski, and H. A. Toliyat, "Predictive current control of voltage source inverters," *IEEE Trans. Ind. Electron.*, vol. 51, no. 3, pp. 585–593, June 2004.
- [8] G. H. Bode, P. C. Loh, M. J. Newman, and D. G. Holmes, "An improved robust predictive current regulation algorithm," *IEEE Trans. Ind. Appl.*, vol. 41, no. 6, pp. 1720–1733, Nov./Dec. 2005.
- [9] H. M. Kojabadi, B. Yu, I. A. Gadoura, L. Chang, and M. Ghribi, "A novel DSP-based current-controlled PWM strategy for single phase grid connected inverters," *IEEE Trans. Power Electron.*, vol. 21, no. 4, pp. 985–993, July 2006.
- [10] P. C. Krause, *Analysis of Electric Machinery*. New York: McGraw-Hill Inc., 1986.
- [11] H. Akagi, Y. Kanazawa, and A. Nabae, "Instantaneous reactive power compensators comprising switching devices without energy storage components," *IEEE Trans. Ind. Appl.*, vol. IA-20, no. 3, pp. 625–630, May/June 1984.
- [12] K. J. Åström and B. Wittenmark, *Computer-Controlled Systems. Theory and Design*, 3rd ed., Prentice-Hall International, Inc., 1997.
- [13] G. Franklin and J. Powell, *Digital Control of Dynamic Systems*. Massachusetts: Addison-Wesley, 1980.
- [14] J. M. Maciejowski, *Multivariable Feedback Design*. Addison-Wesley, 1989.
- [15] K. J. Åström, *Introduction to Stochastic Control Theory*. New York: Dover, 2006.